The Company of Biologists

RESEARCH REPORT

Early perturbation of Wnt signaling reveals patterning and invagination-evagination control points in molar tooth development

Rebecca Kim[1], Tingsheng Yu[1], Jingjing Li[2], Jan Prochazka[3], Amnon Sharir[1,*], Jeremy B. A. Green[1,2,‡] and Ophir D. Klein[1,4,‡]

ABSTRACT

Tooth formation requires complex signaling interactions both within the oral epithelium and between the epithelium and the underlying mesenchyme. Previous studies of the Wnt/β-catenin pathway have shown that tooth formation is partly inhibited in loss-of-function mutants, and gain-of-function mutants have perturbed tooth morphology. However, the stage at which Wnt signaling is first important in tooth formation remains unclear. Here, using an *Fgf8*-promoter-driven, and therefore early, deletion of β-catenin in mouse molar epithelium, we found that loss of Wnt/β-catenin signaling completely deletes the molar tooth, demonstrating that this pathway is central to the earliest stages of tooth formation. Early expression of a dominant-active β-catenin protein also perturbs tooth formation, producing a large domed evagination at early stages and supernumerary teeth later on. The early evaginations are associated with premature mesenchymal condensation marker, and are reduced by inhibition of condensation-associated collagen synthesis. We propose that invagination versus evagination morphogenesis is regulated by the relative timing of epithelial versus mesenchymal cell convergence regulated by canonical Wnt signaling. Together, these studies reveal new aspects of Wnt/β-catenin signaling in tooth formation and in epithelial morphogenesis more broadly.

KEY WORDS: Tooth development, Epithelial invagination, Morphogenesis, Wnt signaling, Mouse

INTRODUCTION

Developing mouse molars have long served as a model to study epithelial morphogenesis because they are simple in structure and can be easily manipulated *ex vivo* (Thesleff and Sharpe, 1997). The first morphological sign of mouse molar development is a localized thickening of the dental epithelium into a placode at embryonic day (E)11.5 (Fig. 1A). The molar epithelium at this stage consists of distinct cell populations, including anterior *Shh*-expressing cells

that form a transient signaling center and more posteriorly located *Fgf8*-expressing molar epithelial progenitors that will form the definitive molar (Prochazka et al., 2015). As the placode grows, it invaginates into the underlying mesenchyme and folds into a tooth bud and then a cap-shaped structure. Concurrently, dental mesenchyme begins to condense around the bud (reviewed by Yu and Klein, 2020 and Tucker and Sharpe, 1999), with reciprocal signaling between the epithelium and mesenchyme ensuing.

The role of Wnt/β-catenin signaling in molar development has been the subject of a number of investigations. Hyperactivation of Wnt signaling in the molar epithelium using stabilized β-catenin or deletion of the Wnt inhibitor *Apc*, both driven by Cre recombinase under the keratin 14 (*Krt14*) promoter, led to formation of supernumerary teeth and abnormal deposits of enamel, respectively (Jarvinen et al., 2006; Wang et al., 2009; Liu et al., 2008). Conversely, hypoactivation of the Wnt pathway disrupted tooth development at various stages (Andl et al., 2002; Liu et al., 2008; Sasaki et al., 2005). Both hyperactivation and hypoactivation of Wnt/β-catenin signaling in the mesenchyme resulted in a decrease in tooth number (Chen et al., 2009; Jarvinen et al., 2018). In humans, loss-of-function mutations of the Wnt inhibitors *APC* and *AXIN2* cause hyperdontia and hypo/oligodontia, respectively (Lammi et al., 2004; reviewed by Wang and Fan, 2011). Thus, although it is evident that Wnt/β-catenin signaling is an essential regulator of molar formation, the precise role of the Wnt pathway in early tooth development remains unclear.

We investigated the role of canonical Wnt signaling by inactivating and hyperactivating it at earlier stages of tooth development than in any previous studies. We previously reported *Fgf8* to be strongly expressed in the molar field at the initiation stage (E11.5) (Prochazka et al., 2015). Using the *Fgf8* promoter to genetically manipulate β-catenin (*Ctnnb1*), we dialed the levels of canonical Wnt signaling up or down at earlier time points than possible with the previously used *Krt14* promoter and specifically in the molar placode. Our findings indicate that the Wnt/β-catenin pathway plays an early, crucial role in determining the early patterning of the tooth primordium, while also showing that the level of signaling controls the relative timing of epithelial versus mesenchymal convergence movements that determine the difference between invagination and evagination, revealing this timing as a potential switch between the two forms.

RESULTS

Wnt/β-catenin signaling is crucial for initiating dental epithelial invagination and subsequent tooth formation

Wnt/β-catenin signaling is active in the *Fgf8*-enriched molar epithelium at the initiation stage (E11.5; Fig. S1A). To study the role of the pathway in early tooth development, we abrogated Wnt signaling in the molar epithelium by deleting both copies of *Ctnnb1*

[1]Program in Craniofacial Biology and Department of Orofacial Sciences, University of California, San Francisco, CA 94143, USA. [2]Centre for Craniofacial Regeneration and Biology, King's College London, London, SE1 9RT, UK. [3]Institute of Molecular Genetics of the ASCR, v. v. i., Prumyslova 595, 252 42 Vestec, Czech Republic. [4]Department of Pediatrics and Institute for Human Genetics, University of California, San Francisco, CA 94143, USA.
*Present address: The Institute of Biomedical and Oral Research, Faculty of Dental Medicine, Hebrew University, Jerusalem 9112102, Israel.

‡Authors for correspondence (Jeremy.Green@ucsf.edu, Ophir.Klein@ucsf.edu)

R.K., 0000-0001-8309-9891; J.L., 0000-0003-4435-7573; J.B.A.G., 0000-0002-6102-2620; O.D.K., 0000-0002-6254-7082
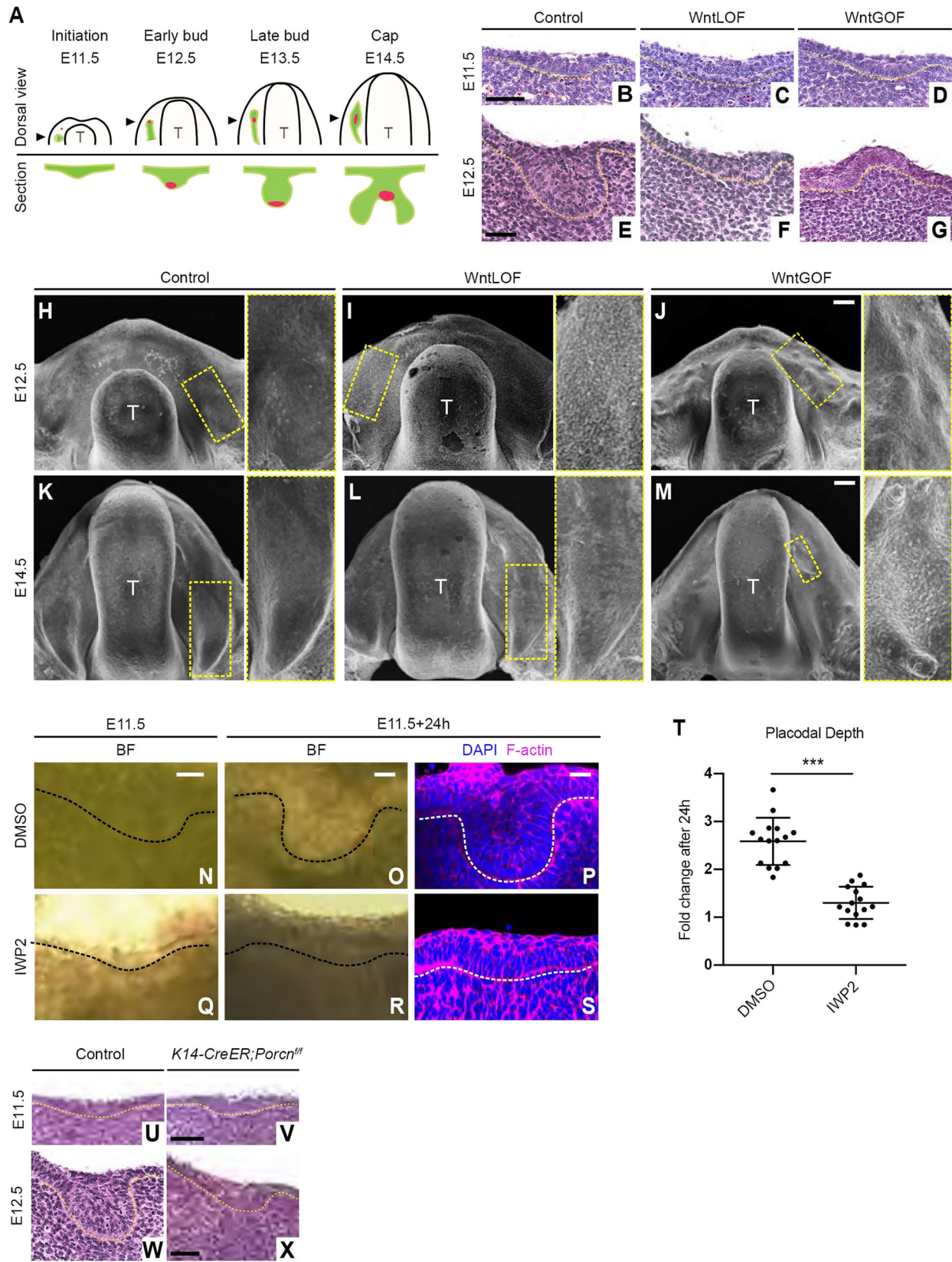
DEVELOPMENT

Fig. 1. Proper Wnt signaling in *Fgf8+* cell population is required for dental epithelial invagination. (A) Schematic of early mouse molar development. Green, *Fgf8*-enriched molar field; red, signaling center. (B-G) Frontal histological sections through molar tooth at E11.5 and E12.5. (H-M) Oral surface view of E12.5 and E14.5 mandibles using scanning electron microscope. T, tongue. Inset (right) shows magnification of yellow boxed area. (N-S) Frontal section of E11.5 mandible cultured for 24 h with DMSO (vehicle) or IWP2. BF, brightfield. (T) Quantification of fold change in placodal depth after IWP2 treatment. Data are mean ±s.d. *n*=15. ***P<0.01 (two-tailed paired Student's *t*-test). (U-X) Histological sections through molar tooth germ at E11.5 and E12.5 in control and *Porcn* mutant. Dashed lines indicate epithelial-mesenchymal border. Scale bars: 50 μm (B-G,N-X); 100 μm (H-J); 200 μm (K-M).

($Fgf8^{CreER}$;$Ctnnb1^{fl/fl}$; hereafter called WntLOF) (Brault et al., 2001; Hoch et al., 2015). In parallel, to hyperactivate the Wnt pathway in the same population, we used a conditional $Ctnnb1$ allele that is resistant to ubiquitin-mediated degradation ($Fgf8^{CreER}$;$Ctnnb1^{\Delta ex3fl/+}$; hereafter called WntGOF) (Harada et al., 1999). In both mutants, tamoxifen was administered intraperitoneally at E10.75 to allow Cre-mediated recombination during the molar initiation stage (E11.5), as previously described (Prochazka et al., 2015).

Histology revealed that at E11.5, the control and both mutants formed a molar placode, characterized by epithelial thickening (Fig. 1B-D). At E12.5, control molar placodes invaginated into the mesenchyme to form a tooth bud (Fig. 1E). In WntLOF, however, the molar primordium did not invaginate noticeably beyond the placodal depth (Fig. 1F). Strikingly, rather than invaginating into the underlying mesenchyme, the WntGOF molar epithelium evaginated into the oral cavity (Fig. 1G).

We used scanning electron microscopy (SEM) to evaluate the WntGOF evagination in 3D. Consistent with the histological sections, WntGOF mutants at E12.5 and E14.5 displayed multiple evaginating structures scattered along the dental and vestibular surfaces instead of the shallow concavity at the molar field as seen in control and WntLOF (Fig. 1H-M). Histology and micro-computed tomography (μCT) of WntLOF and WntGOF mandibles at E18.5 revealed persistence of loss-of-invagination and evagination phenotypes, respectively, with neither mutant yielding any obvious tooth structure (Fig. S1B-D,F-H). Interestingly, the deepest invagination of the molar epithelium in $Fgf8$-driven WntGOF, which is expressed primarily in the molar progenitors, remained only slightly below the level of oral epithelium (Fig. S1D). These phenotypes contrast with those found in previous studies, in which $Krt14$ promoter-driven expression of a stabilized β-catenin throughout the oral epithelium produced hyperinvagination of the epithelium (Järvinen et al., 2006; Liu et al., 2008).

WntGOF caused perinatal lethality, making it impossible to follow development of the evaginating structures into the postnatal period. To circumvent this, the evaginating structures within the diastema (the toothless area between molar and incisor) of E12.5 WntGOF and littermate control mandibles were grown under the kidney capsule of immunocompromised mice for 4 weeks and scanned using μCT. The control explants yielded three molars (two out of three molars shown in Fig. S1I), whereas WntGOF explants gave rise to supernumerary teeth (n=2; Fig. S1J). This is consistent with previous studies showing that Wnt hyperactivation induces supernumerary tooth formation (Järvinen et al., 2006; Liu et al., 2008).

β-Catenin has a dual role in signaling and cell adhesion (Valenta et al., 2012). To determine whether inhibition of Wnt/β-catenin signaling alone is sufficient to produce the WntLOF phenotype, we chemically and genetically perturbed porcupine ($Porcn$), a member of the Wnt pathway essential for Wnt ligand secretion and activity, but not involved in cell-cell adhesion. Wild-type E11.5 mandibular explants were treated with IWP2 to pharmacologically inhibit $Porcn$. After 24 h, the molar placodal depth of explants treated with DMSO (vehicle control) increased 2.63-fold (n=15; s.d.=0.50), whereas the placodal depth in IWP2-treated explant increased just 1.30-fold (n=15; s.d.=0.34) (Fig. 1N-T). Genetic abrogation of $Porcn$ in oral and dental epithelium using $Krt14$-$CreER^{T2}$;$Porcn^{fl/fl}$ also led to a delay in tooth development by E18.5 (Fig. 1U-X). Histological staining of $Porcn$ mandible at E18.5 revealed an enamel organ, suggesting that $in~vivo$ the mutant can still form a tooth germ, at least up to early bell stage (Fig. S1E). This is consistent with a previous study that reported missing and hypoplastic teeth in $Krt14$-Cre; $Porcn^{fl/fl}$ mouse mutants (Liu et al., 2012). Overall, the

$Krt14$-$CreER^{T2}$;$Porcn^{fl/fl}$ phenotype is consistent with the literature on Wnt hypomorphs in tooth showing partial disruption of tooth formation, and its similarity to our WntLOF phenotype at early stages confirms that the latter is likely due to a loss of canonical signaling and not primarily loss of β-catenin-dependent cell adhesion.

In Wnt mutants, expression of odontogenic genes, cell proliferation and survival are perturbed

We next assessed the expression levels of representative members of the canonical pathways involved in odontogenesis. Whole-mount $in~situ$ hybridization of E11.75 mandibles (Fig. S2A-U) revealed that genes expressed in dental epithelium that are crucial for proper tooth development ($Fgf8$, Shh, $Fgf4$ and $Bmp4$) were downregulated in WntLOF and upregulated in WntGOF. Because the controls for WntLOF and WntGOF were highly similar, representative controls are shown for each probe. Upregulation and downregulation of $Wnt10b$ expression in WntGOF and WntLOF, respectively, suggested an autoregulatory feedback loop. At E12.5, dental epithelial markers that were expressed at E11.75 were reduced in both control and WntLOF molar epithelium but persisted in the evaginating structures in WntGOF (Fig. S2V-DD,KK-PP). $Msx1$ and $Barx1$, which are expressed in dental mesenchyme, were downregulated in WntLOF and colocalized with the evaginating mesenchyme of WntGOF mutants, suggesting that the evaginating structures will give rise to tooth structures (Fig. S2J-O,EE-JJ).

Wnt/β-catenin signaling regulates proliferation in a number of contexts (reviewed by Clevers, 2006). To determine whether the mutants had changes in proliferation or apoptosis, EdU and TUNEL staining were performed (Fig. 2A-Q). In E11.5 WntLOF molar epithelium, the proportion of EdU-labeled cells significantly decreased, whereas the number of TUNEL-labeled apoptotic cells significantly increased (Fig. 2B,E,H,K,N-Q). Interestingly, EdU-labeled cells were also increased in the WntLOF molar mesenchyme. No significant difference was detected in EdU or TUNEL labeling in WntGOF mutants, in both epithelium and mesenchyme (Fig. 2C,F,I, L,N-Q). This indicates that Wnt/β-catenin signaling is essential for proliferation and survival of molar epithelial cells to form tooth germ, but is insufficient to perturb either mechanism when hyperactivated, suggesting that other cellular mechanisms contribute to evagination in WntGOF. In addition, there was an increase in mesenchymal cell density in both WntLOF and WntGOF mesenchyme at E12.5 (Fig. 2M).

Wnt/β-catenin signaling is required for the convergence of suprabasal cells during molar epithelial invagination

To investigate whether additional cell behaviors are altered when Wnt signaling is perturbed, we performed time-lapse microscopy on explant culture tissue slices. The molar placodes formed at the start of imaging (E11.5) had similar morphology in WntLOF and control (Fig. 2R,U; Movies 1 and 2). In controls, movement of epithelial cells towards the center of the placode was observed within 9 h as the width decreased and the depth increased (Fig. 2R-T), consistent with previous work (Panousopoulou and Green, 2016). This cell convergence was not observed in WntLOF, resulting in a shallower placode (Fig. 2U-W). We were not able to image the evagination process because the presumptive evaginating sites were impossible to predict.

F-actin enrichment is associated with active cell shape changes and migration (Stricker et al., 2010), so F-actin expression was examined to assess whether the placodal cell convergence could be driven by the active cytoskeleton of the epithelial cells themselves, as opposed to passive movement caused by external forces. At
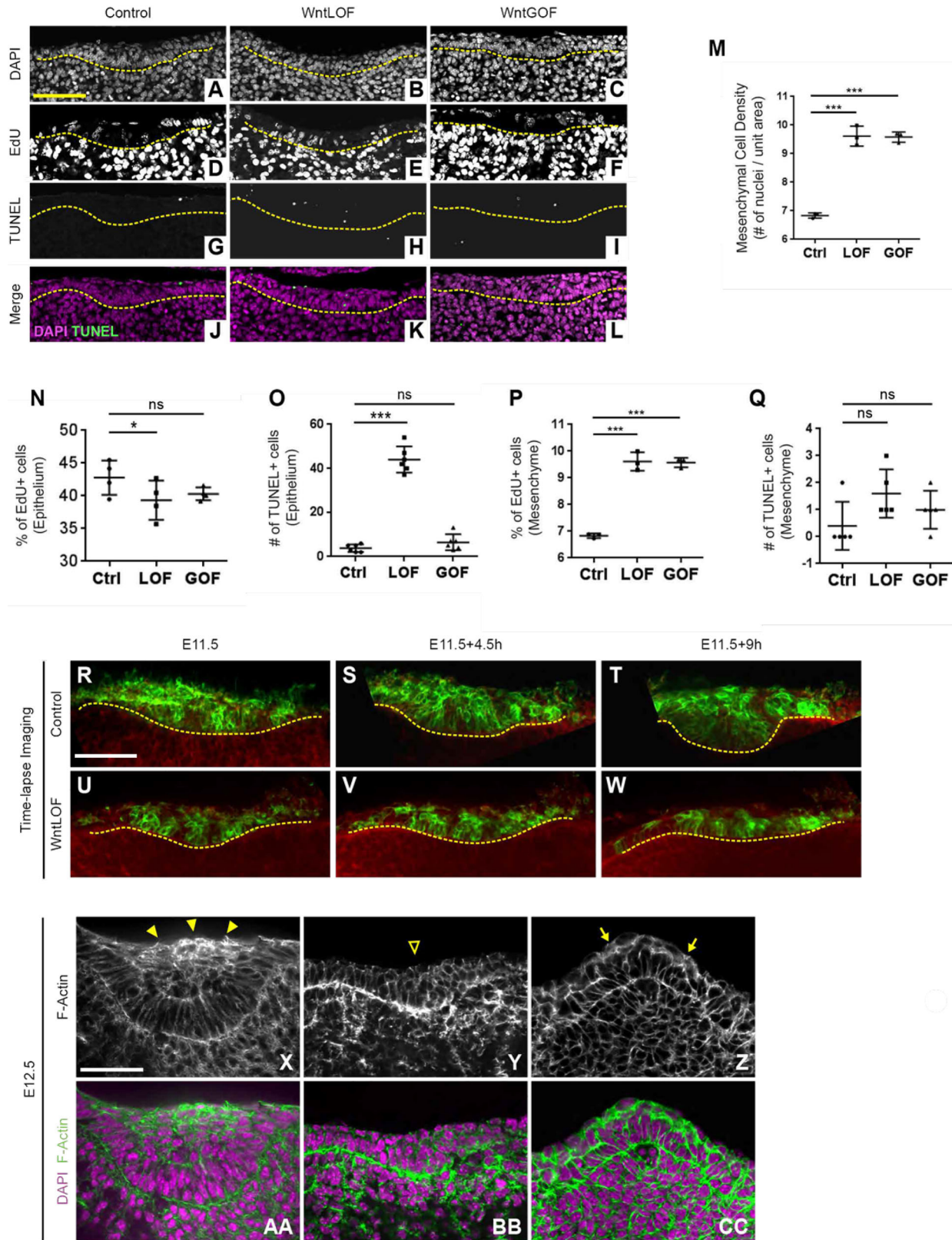
Fig. 2. Wnt signaling is required for cell proliferation and survival, and medial movement of suprabasal cells. (A-L) Representative image of DAPI, EdU and TUNEL staining in molar tooth germ at E11.5. (M) Quantification of nuclear density in E12.5 molar mesenchyme. (N-Q) Quantification of the average percentage of EdU-stained cells and total number of TUNEL-stained cells in seven sequential sections. (R-W) Time lapse imaging of E11.5 mandible slice culture of control and WntLOF. Green, dental epithelial cells; red, non-dental epithelial cells. Yellow dashed line, epithelial-mesenchymal border. (X-CC) F-actin staining of presumptive tooth germ at E12.5. Filled arrowhead, F-actin enrichment; open arrowhead, absence of F-actin enrichment; arrow, cortical-actin-like F-actin expression. Data are mean±s.d. For M-Q, *$P<0.05$. ***$P<0.01$ (two-tailed paired Student's t-test). ns, statistically not significant. Scale bars: 50 μm.

E11.5, before invagination, there was no F-actin enrichment in the molar placodes of the control and both mutants (Fig. S3C-H). By E12.5, the suprabasal layer of controls was highly enriched with F-actin (Fig. 2X,AA). In contrast, WntLOF molar epithelium did not exhibit F-actin enrichment, suggesting the loss of canopy formation (Fig. 2Y,BB). WntGOF epithelium exhibited an increase in F-actin expression, but this appeared similar to diffuse cortical actin (Fig. 2Z,CC), rather than the cable-like expression observed in the suprabasal layer of invaginating molar epithelium (Fig. 2X).

Evaginating mesenchyme in WntGOF mutants exhibits compromised epithelial integrity and premature mesenchymal condensation

In skin, γ-catenin can compensate for β-catenin-mediated cell adhesion (Huelsken et al., 2000, 2001). Indeed, γ-catenin was expressed throughout the WntLOF dental epithelium, whereas it was enriched in suprabasal layer in control, suggesting that γ-catenin may substitute for the adhesion function upon loss of β-catenin (Fig. 3A,B,D,E). Interestingly, there was reduced
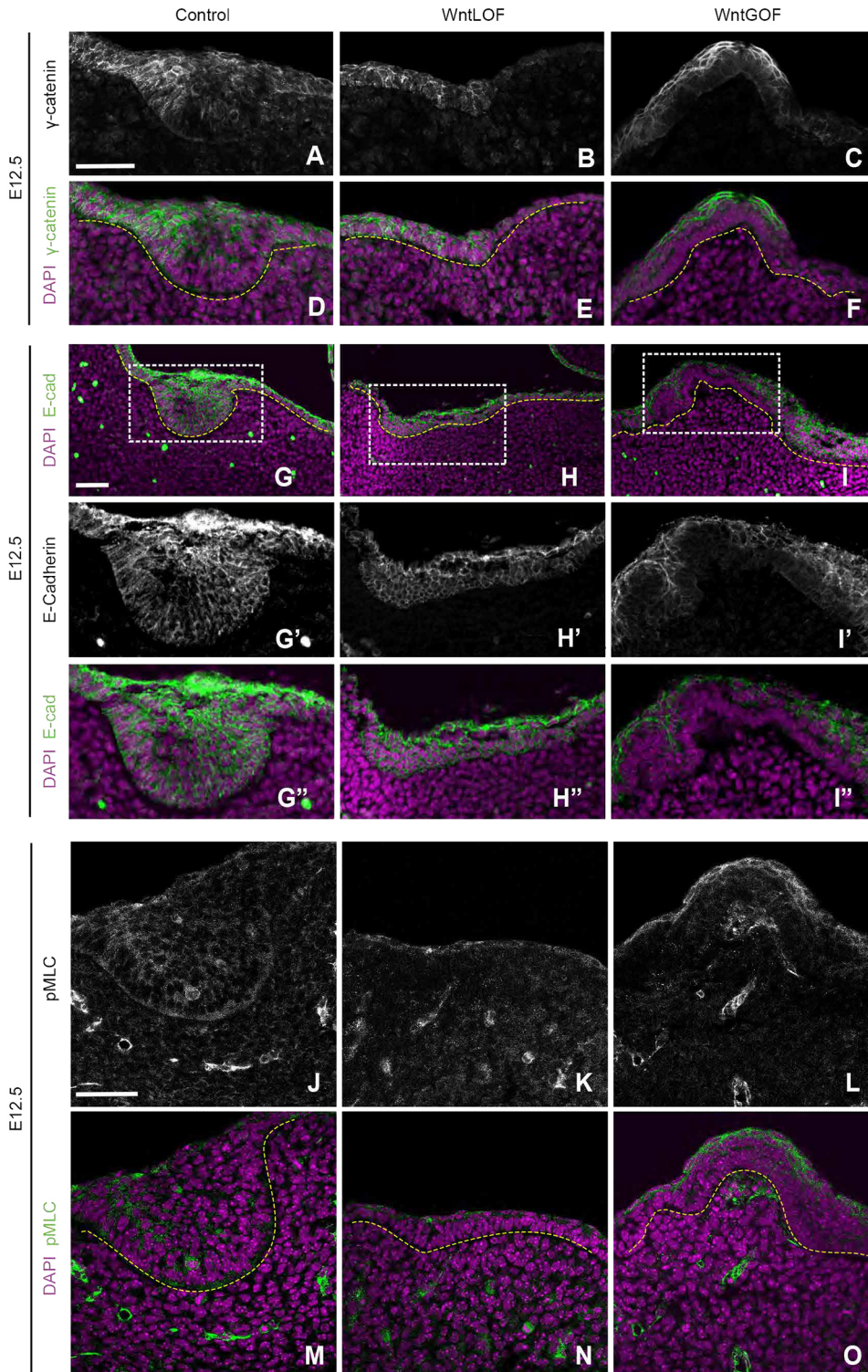

Fig. 3. Reduced epithelial actin bundles and E-cadherin expression in evaginating structure. (A-F) γ-Catenin staining of presumptive tooth germ in control, WntLOF and WntGOF at E12.5. (G-I″) E-cadherin expression in E12.5 presumptive tooth germ. G′,G″, H′,H″ and I′,I″ show magnifications of boxed areas in G,H and I, respectively. (J-O) pMLC expression in E12.5 presumptive tooth germ. Yellow dashed line, epithelial-mesenchymal border. Scale bars: 50 μm.

expression of γ-catenin within the evaginating epithelium in WntGOF (Fig. 3C,F).

E-cadherin is another essential component of adherens junctions (van Roy and Berx, 2008) that can be downregulated upon activation of Wnt/β-catenin signaling (ten Berge et al., 2008; Jamora et al., 2003). The expression pattern of E-cadherin in control and WntLOF was comparable with that of γ-catenin (Fig. 3G-G″,H-H″). Also consistent with γ-catenin expression, the E-cadherin expression in evaginating epithelium of WntGOF was reduced and localized to the suprabasal layer (Fig. 3I-I″), suggesting a subtle reduction of cell adhesion and/or epithelial integrity in the evaginating epithelium. Apical location of the Golgi, as marked by GM130, relative to the nucleus of the basal cells indicates that the apicobasal polarity is maintained in WntGOF (Fig. S3A,B; Debnath et al., 2002).

We next considered whether the evagination in the WntGOF mutant might be driven not by the epithelium itself, but instead by underlying mesenchyme pushing the epithelium outward into the oral cavity. We asked whether extracellular matrix (ECM) plays a role in evagination, studying collagen VI as a representative marker. Collagen VI expression can be induced by dental mesenchymal condensation and may play a role in stabilizing the condensed mesenchyme (Mammoto et al., 2015). Indeed, there was an increase in mesenchymal cell density in the evaginating mesenchyme

compared with that in control at E12.5 (Fig. 2M). In control dental mesenchyme, collagen VI expression was restricted to the basement membrane at E12.5, when the dental mesenchymal condensation initiates (Fig. 4A,B). By E14.5, collagen VI expression was strongly enriched within the condensed dental mesenchyme (Fig. 4E,F). In WntGOF, collagen VI expression was already observed in the evaginating mesenchyme at E12.5 and persisted until E14.5 (Fig. 4C,D,G,H). Thus, the evagination process in WntGOF may be coupled to premature mesenchymal condensation, as well as ectopic expression of collagen VI. In addition, non-muscle myosin II has been shown to be involved in condensation of the collagenous ECM in the mouse intestine (Hughes et al., 2018). In the control molar mesenchyme, there was circumferential expression of phospho-myosin light chain (pMLC) that parallels the curvature of the basement membrane (Fig. 3J,M), whereas this expression was absent in the WntLOF mesenchyme (Fig. 3K,N). Interestingly, the pMLC expression in the WntGOF embryos showed myosin activity in the evaginating mesenchyme (Fig. 3L,O).

To test whether increased collagenous ECM contributes to evagination, we pharmacologically inhibited collagen synthesis in E11.5 WntGOF and control mandibles. Each mandible was bisected, and one hemimandible treated with the collagen synthesis inhibitor Mithramycin A (Mit A) (Blume et al., 1991; Ihn et al., 2001) and the other with vehicle (DMSO) (Fig. 4I). After 48 h, Mit
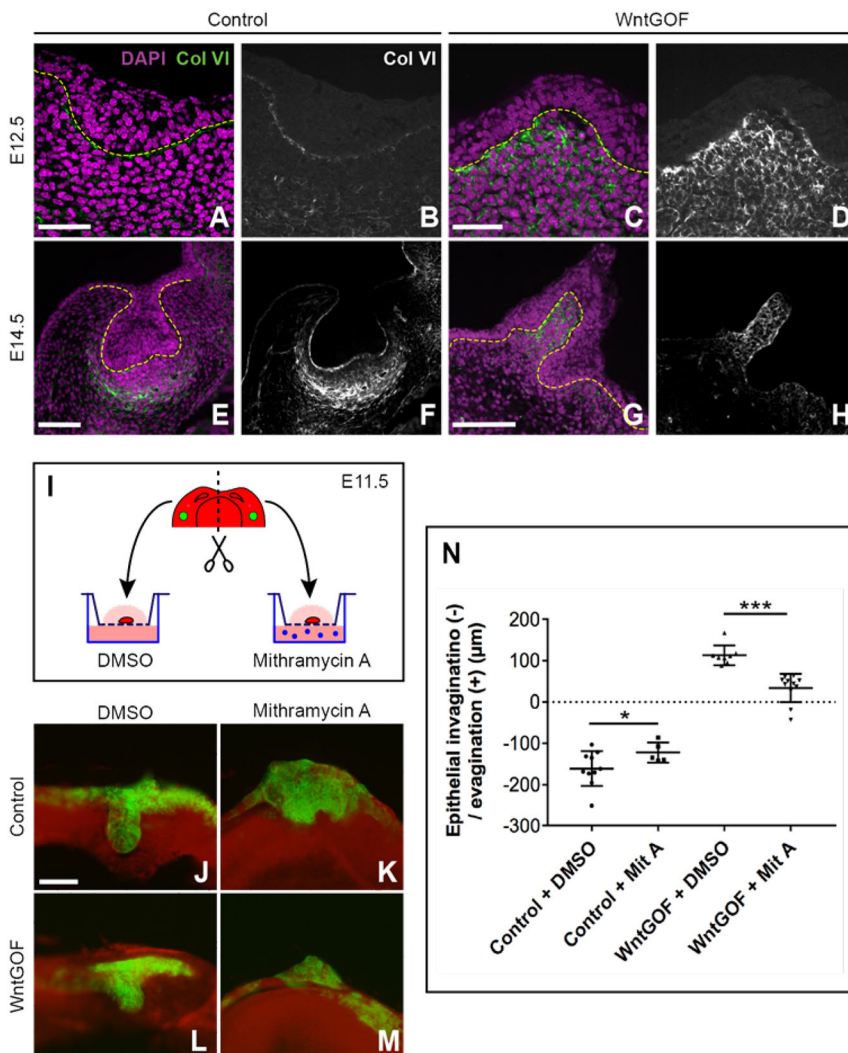

Fig. 4. Premature collagen VI expression is observed in evaginating structures and contributes to evagination phenotype. (A-H) Immunofluorescence of collagen VI (Col VI) at E12.5 and E14.5 in control and WntGOF. Yellow dashed line, epithelial-mesenchymal border. (I) Schematic of explant culture experiment. (J-M) Frontal section of presumptive tooth germs after 48 h. Green, dental epithelial cells; red, non-dental epithelial cells. (N) Quantification of fold change in placodal depth after Mit A treatment. Data are mean±s.d. *P<0.05, ***P<0.01 (two-tailed paired Student's t-test). Scale bars: 50 μm.

A treatment partially prevented both invagination of control molar placode and evagination in WntGOF. However, the decrease in height of evagination in WntGOF was significantly greater than the depth reduction of molar epithelial invagination in control (Fig. 4J-N). As expected, there was a decrease in overall collagen VI expression in the explants treated with Mit A (Fig. S3I-L). This suggested that the premature and dysregulated accumulation of ECM proteins, such as collagen VI, promotes evagination in WntGOF mutants through increasing local mesenchymal stiffness along with premature increased cell density. One potential caveat to these results is that although it is frequently used to inhibit collagen synthesis, Mit A may affect other biological processes as well.

DISCUSSION

An accumulation of tooth mutant phenotypes has, over the years, established that Wnt/β-catenin signaling is an integral part of the regulatory signaling network of tooth development. However, exactly how Wnt/β-catenin signaling regulates tooth development – not just the signaling but also the morphogenesis – has remained unclear. Previous studies have been carried out by either global or pan-epithelial manipulation of the Wnt/β-catenin pathway, which resulted in blockage of tooth development at various late stages. The discrepancy in phenotypes resulting from the perturbation of the same pathway has obscured the precise role of Wnt signaling in tooth development. The reason for the different phenotypes from perturbation of the same pathway is likely due to the difference in the temporospatial specificity of the Cre drivers. Here, we found that abrogating Wnt/β-catenin signaling in *Fgf8*-enriched molar epithelium almost completely prevented the molar placode from invaginating into the underlying mesenchyme, thereby resulting in near deletion of the tooth germ. This indicates that Wnt/β-catenin signaling is essential for epithelial invagination at the earliest stages. We observed several cellular processes that may contribute to the WntLOF phenotype, including a decrease in cell proliferation and survival. Live imaging data revealed that the overall movement of molar epithelial cells towards the midline of the placode was lost upon abrogation of the Wnt pathway, which may drive the WntLOF phenotype. Our data also indicate that the Wnt pathway lies upstream of SHH, FGF and BMP signaling, which in turn may mediate the mutant phenotypes (Li et al., 2016).

The evaginating tooth germ in the WntGOF mutants resembles those found in early tooth development of paddlefish, alligators and turtles (Kozawa et al., 2005; Smith et al., 2015; Tokita et al., 2013). It also resembles the evaginations observable, but rarely noted, that raise feather buds and some hair follicles such as the vibrissae (whiskers) above surrounding skin. Our findings suggest that premature mesenchymal condensation in WntGOF may push the epithelium outward as it compacts around the presumptive tooth sites.

The mechanisms underlying mesenchymal condensation are not fully understood, including the temporal relationships between cell density, tissue stiffness and cell movement. In addition to cell compaction, it is possible that other features of mesenchymal condensation, such as production of ECM, also play a role. Premature collagen VI expression in WntGOF suggests dysregulated mesenchymal condensation. Indeed, there was a significant increase in cell density within the evaginating mesenchyme of WntGOF at E12.5 compared with that of control dental mesenchyme. Interestingly, collagen VI has also been reported to be associated with Bethlem myopathy and Ullrich congenital muscular dystrophy in humans (Baker et al., 2007, 2005). These patients have irregular, crowded dentition, further suggesting its role

as an ECM protein in dental mesenchyme during tooth development. Furthermore, mesenchymal condensation has also been observed in other organs that develop through evagination, such as feather buds and intestinal villi (Widelitz et al., 2003; Hughes et al., 2018; Shyer et al., 2017). A simple change in the timing of cell convergence in the epithelium and cell convergence (condensation) in the mesenchyme could act as an evolutionary switch between evagination and invagination, regulated as simply as by changing the strength of canonical Wnt signaling.

Lastly, it is notable that the location of evagination sites in WntGOF appeared to be stochastic, as opposed to predictable and sequential sites of molar tooth germ in control. One simple explanation could be that the elevated Wnt signaling promotes the survival and proliferation of *Fgf8+* cells, a well-known role of Wnt signaling in various tissue contexts. However, although the ectopic evagination locations appeared random, they were always well-spaced. These phenotypes are consistent with a residual periodic reaction-diffusion (RD)-type mechanism. Spatial and temporal patterning of tooth germs has long been theorized to be patterned via an RD system (Murray and Kulesa, 1996; Sadier et al., 2019). Indeed, members of the Wnt pathway have been shown to pattern spacing via RD in the hair follicle (Sick et al., 2006) and, more recently, experiments and modeling have reinforced this idea for molar patterning (Sadier et al., 2019). If this is the case, then our results indicate that Wnt is a likely participant in the core RD network that initiates the tooth germ, and the proper balance of signaling through this network ultimately dictates whether an invagination or an evagination will form. Through control of this essential early step in tooth formation, titration of levels of Wnt signaling ensures that subsequent stages of morphogenesis have the correct building blocks to work with.

MATERIALS AND METHODS
Mouse genetics

All animal experiments were performed in accordance with the guidelines established by Institutional Animal Care and Use Committee (IACUC) and Laboratory Animal Resource Center (LARC) of University of California, San Francisco, CA, USA. The following mouse strains were used: C57BL/6J (Jackson Laboratory: 000664); *Fgf8^{CreER}* (Hoch et al., 2015); *Krt14-CreER^{T2}* (MGI: 2177426); *Porcn^{flox}* (MGI: 1890212); *Ctnnb1^{Δex3fl/+}* (MGI: 1858008); *Ctnnb1^{flox}* (MGI: 2148567); *R26^{mT/mG}* (MGI: 3716464); *BAT-GAL* (MGI: 3697064); *Foxn1^{nu}* (immunocompromised mice; Jackson Laboratory: 007850). For generation of embryos and kidney capsule transplant, 6- to 8-week-old animals were used for breeding. Tamoxifen (0.2 mg/g of body weight) was administered via intraperitoneal (IP) injection to pregnant dams at E10.75 to induce genetic recombination by the initiation stage (E11.5). Each experiment was performed at least three times with different embryos. The following developmental features were used as references to confirm the stages of the harvested embryos: E11.5 – visible auditory hillocks, round anterior foot plates, fusion of two lateral lingual swellings; E12.5 – interdigital indentations without clear separation of digits, separation of the tongue from the oral epithelium.

EdU and TUNEL staining and quantification

The mice at E11.5 of pregnancy were administered with EdU (Invitrogen, C10637; 1 mg/25 g body weight) via IP injection 1 h before euthanasia. All the harvested embryos were fixed in 4% paraformaldehyde (PFA) at 4°C at the same time immediately after decapitation. Following overnight fixation, mandibles were isolated and sectioned for subsequent analysis. EdU detection was performed according to standard protocol provided by the EdU detection kit (Thermo Fisher Scientific, C10338). The total number of nuclei and the EdU+ nuclei were counted in seven sequential sections, and the proportion of EdU+ nuclei to the total number of nuclei was used for quantitative analyses. As for the mesenchyme, region of analysis was

defined to include five to six layers of mesenchymal cells from the basement membrane surrounding the invaginating epithelium.

For TUNEL staining, sections were deparaffinized, rehydrated and incubated in 0.1% trypsin solution at 37°C for 14 min. The *In Situ* Cell Death Detection Kit, TMR red (Roche, 12156792910) was used according to manufacturer's instructions. Positive and negative controls were included per manufacturer's instruction. The total number of TUNEL-stained nuclei from seven sequential sections was counted for quantitative analyses. The EdU and TUNEL counts were comparable between the WntLOF control and WntGOF controls and were thus pooled for counting.

To calculate mesenchymal cell density, the mesenchymal area for counting was defined as explained above, and all of the nuclei within the defined parameter were counted. Cell density was calculated by dividing the number of nuclei by a defined area, which is automatically calculated by Fiji software.

X-gal staining and section *in situ* hybridization

Mandibles were harvested from BAT-GAL embryos at E11.5 and fixed in Mirsky's fixative (National Diagnostics) overnight and subsequently stained in X-Gal solution. Stained samples were rinsed, post-fixed in 4% PFA and paraffin-sectioned for subsequent *in situ* hybridization. *In situ* hybridization to detect *Fgf8* expression was performed using DIG-labeled probes using a protocol modified from Riddle et al. (1993). Modifications are detailed in the 'Whole-mount *in situ* hybridization' section.

Kidney capsule graft

The portion of the mandibles containing the evaginating structures was dissected from E12.5 WntGOF embryos and transplanted under the renal capsule of immunocompromised mice ($Foxn1^{nu}$). The equivalent region of littermate controls, including the molar tooth germs, were used as controls. The analgesics were administered according to the IACUC guidelines. The mice were anesthetized by isoflurane inhalation. Aseptic techniques were practiced for surgery. A longitudinal incision of 1-1.5 cm was made to exteriorize the kidney. One tooth germ was transplanted under the kidney capsule per animal. The peritoneum and skin were closed with suture. The mice were then placed under a heat lamp for recovery and monitored until fully awake. The mice were euthanized for retrieval of the grafts for analyses 4 weeks post-surgery, and the grafts were scanned using μCT.

Micro-computed X-ray tomography

Samples were scanned using MicroXCT-200 (Carl Zeiss Microscopy). The harvested renal grafts were gradually dehydrated to 70% ethanol and scanned at 40 kV and 200 μA. We took 800 projection images at a total integration time of 12 s with linear magnification of 4 and a pixel size of 5.4 μm. For imaging of the E18.5 heads, samples were additionally soaked in phosphotungstic acid overnight to differentially stain soft tissues as described in Metscher (2009) and scanned at 60 kV and 200 μA. We took 1200 projection images at a total integration time of 4 s, with linear magnification of 4 and a pixel size of 4.4μm. Images were analyzed using Avizo (FEI).

Whole-mount *in situ* hybridization

Embryonic mandibles were fixed in 4% PFA overnight at 4°C. *In situ* hybridization was performed using a protocol modified from Riddle et al. (1993). Prior to *in situ* hybridization, all samples were dehydrated through graded methanol and stored at −20°C until further use. Immediately prior to *in situ* hybridization, samples were gradually rehydrated to DEPC-treated PBST (PBS with 0.1% Tween 20) and incubated in 6% hydrogen peroxide. The subsequent steps are as described by Riddle et al. (1993).

The plasmids for the generation of RNA probes were kind gifts of Drs I. Thesleff (University of Helsinki, Finland; Wnt10b), G. Martin (University of California, San Francisco, USA; *Fgf8*, *Shh*, *Msx1*, *Fgf4* and *Bmp4*) and T. Mitsiadis (University of Zurich, Switzerland; *Barx1*). To generate antisense probes, plasmids were linearized with the appropriate restriction enzymes (RE) and transcribed using RNA polymerase (RNAP) with RNA-DIG labeling mix (Roche). RNA probes were precipitated and resuspended in RNAase-free water. DIG-labeled RNA probes were transcribed *in vitro* from plasmids containing: *Wnt10b*, *Fgf8*, *Shh*, *Msx1*, *Barx1*, *Fgf4* and *Bmp4*.

Live imaging

The $R26^{mT/mG}$ reporter was crossed into $Fgf8^{CreER}$ (control) and $Fgf8^{CreER}$; $Ctnnb1^{fl/fl}$ (WntLOF) to visualize molar epithelial cells. Embryonic mandibles were harvested at E11.5. From each mandible, two incisions near the lateral borders of the tongue were introduced to remove tongue primordium and generate two hemi-mandibles. The hemi-mandibles were manually sliced to generate a frontal section through the molar placode for imaging. The explants were embedded and cultured in 0.3% low melting point agarose medium for the entire duration of the imaging as described in Prochazka et al., 2015. Live imaging was performed using a CSU-X1 Yokogawa spinning disk confocal unit on an inverted Zeiss Observer Z1 microscope.

Immunofluorescence and Phalloidin staining

Immunofluorescence was performed on paraffin sections and cryosections. Paraffin sections were de-paraffinized and rehydrated. Antigen retrieval was performed by sub-boiling slides in a microwave for 15 min in a citrate buffer (pH 6.2) containing 10 mM citric acid, 2 mM EDTA and 0.05% Tween-20. Samples were blocked in animal-free blocker (Vector Laboratories, SP-5030) supplemented with 2.5% heat-inactivated goat serum, 0.02% SDS and 0.1% Triton X-100. Anti-collagen VI (Abcam, ab182744), anti-pMLC (Abcam, ab2480), anti- γ-catenin (Abcam, ab184919), anti-E-cadherin (Cell Signaling Technology, 3195S) and anti-GM130 (Cell Signaling Technology, 2296S) primary antibodies were used. All of the antibodies were diluted 1:300 in the same blocking solution without serum.

For Phalloidin staining, embryos were fixed in 4% PFA overnight at 4°C, graded to 30% sucrose, embedded in OCT and cryo-sectioned. Sections were stained with Alexa Fluor™594 (Thermo Fisher Scientific, A12381) according to the manufacturer's protocol. DAPI (Invitrogen, D1306) was used to stain nuclei for immunofluorescence and Phalloidin staining. All of the images were acquired using CSU-X1 Yokogawa spinning disk confocal unit on an inverted Zeiss Observer Z1 microscope.

Histology

Embryonic mandibles were fixed in Bouin's fixative overnight at room temperature, paraffin-sectioned, dehydrated through graded ethanol concentrations, deparaffinized with Histoclear (National Diagnostics), rehydrated through an ethanol gradient, stained with Hematoxylin and Eosin, dehydrated through an ethanol gradient, incubated in histoclear, and mounted using Permount (Fisher Scientific).

SEM

Harvested embryonic mandibles were fixed in 4% PFA and gradually dehydrated to 100% ethanol. Samples were subject to critical point drying, mounted to SEM sample stub and sputtered with gold-palladium. Scanning electron micrographs were obtained using a JEOL JCM-5000 Neoscope Scanning Electron Microscope. All SEM was performed at the University of California, San Francisco DRC Microscopy core.

Pharmacological inhibition assay

Embryonic mandibles were harvested at E11.5 and bisected. The left hemimandible was treated with DMSO and the right side with 250 nM Mit A (Tocris, #1489). Each hemimandible was embedded in Matrigel (356231, Corning) on a cell culture insert (Millicell) in a 12-well plate. Explants were cultured at the interface of air and media, comprising DMEM/F12 (Gibco), 20% fetal bovine serum, 1% glutamine, and 1% penicillin/streptomycin, at 37°C and 5% CO_2. After 48 h of culture, explants were rinsed, fixed with 4% PFA and embedded in 6% low-melting agarose (Invitrogen). Fixed samples were then vibratome-sectioned at thickness of 50 μm and imaged using a Leica DMi8 S platform live cell microscope. The depth of dental epithelial invagination or evagination was measured from the center of the suprabasal layer vertically to the expanded dental epithelium.

Statistical analysis

Data are expressed as mean±s.d. Two-tailed paired Student's *t*-tests were used for EdU and TUNEL staining, mesenchymal cell density, IWP2 data and Mit A inhibition data.

References

Andl, T., Reddy, S. T., Gaddapara, T. and Millar, S. E. (2002). WNT signals are required for the initiation of hair follicle development. *Dev. Cell* **2**, 643-653. doi:10.1016/S1534-5807(02)00167-3

Baker, N. L., Morgelin, M., Peat, R., Goemans, N., North, K. N., Bateman, J. F. and Lamande, S. R. (2005). Dominant collagen VI mutations are a common cause of Ullrich congenital muscular dystrophy. *Hum. Mol. Genet.* **14**, 279-293. doi:10.1093/hmg/ddi025

Baker, N. L., Morgelin, M., Pace, R. A., Peat, R. A., Adams, N. E., Gardner, R. J., Rowland, L. P., Miller, G., De Jonghe, P., Ceulemans, B. et al. (2007). Molecular consequences of dominant Bethlem myopathy collagen VI mutations. *Ann. Neurol.* **62**, 390-405. doi:10.1002/ana.21213

Brault, V., Moore, R., Kutsch, S., Ishibashi, M., Rowitch, D. H., McMahon, A. P., Sommer, L., Boussadia, O. and Kemler, R. (2001). Inactivation of the (β)-catenin gene by Wnt1-Cre-mediated deletion results in dramatic brain malformation and failure of craniofacial development. *Development* **128**, 1253-1264. doi:10.1242/dev.128.8.1253

Blume, S. W., Snyder, R. C., Ray, R., Thomas, S., Koller, C. A. and Miller, D. M. (1991). Mithramycin inhibits Sp1 binding and selectively inhibits transcriptional activity of the dihydrofolate reductase gene in vitro and in vivo. *J. Clin. Invest.* **88**, 1613-1621. doi:10.1172/JCI115474

Chen, J., Lan, Y., Baek, J. A., Gao, Y. and Jiang, R. (2009). Wnt/beta-catenin signaling plays an essential role in activation of odontogenic mesenchyme during early tooth development. *Dev. Biol.* **334**, 174-185. doi:10.1016/j.ydbio.2009.07.015

Clevers, H. (2006). Wnt/beta-catenin signaling in development and disease. *Cell* **127**, 469-480. doi:10.1016/j.cell.2006.10.018

Debnath, J., Mills, K. R., Collins, N. L., Reginato, M. J., Muthuswamy, S. K. and Brugge, J. S. (2002). The role of apoptosis in creating and maintaining luminal space within normal and oncogene-expressing mammary acini. *Cell* **111**, 29-40. doi:10.1016/S0092-8674(02)01001-2

Harada, N., Tamai, Y., Ishikawa, T., Sauer, B., Takaku, K., Oshima, M. and Taketo, M. M. (1999). Intestinal polyposis in mice with a dominant stable mutation of the beta-catenin gene. *EMBO J.* **18**, 5931-5942. doi:10.1093/emboj/18.21.5931

Hoch, R. V., Clarke, J. A. and Rubenstein, J. L. (2015). Fgf signaling controls the telencephalic distribution of Fgf-expressing progenitors generated in the rostral patterning center. *Neural Dev.* **10**, 8. doi:10.1186/s13064-015-0037-7

Huelsken, J., Vogel, R., Brinkmann, V., Erdmann, B., Birchmeier, C. and Birchmeier, W. (2000). Requirement for beta-catenin in anterior-posterior axis formation in mice. *J. Cell Biol.* **148**, 567-578. doi:10.1083/jcb.148.3.567

Huelsken, J., Vogel, R., Erdmann, B., Cotsarelis, G. and Birchmeier, W. (2001). β-Catenin controls hair follicle morphogenesis and stem cell differentiation in the skin. *Cell* **105**, 533-545. doi:10.1016/S0092-8674(01)00336-1

Hughes, A. J., Miyazaki, H., Coyle, M. C., Zhang, J., Laurie, M. T., Chu, D., Vavrusova, Z., Schneider, R. A., Klein, O. D. and Gartner, Z. J. (2018). Engineered Tissue folding by mechanical compaction of the mesenchyme. *Dev. Cell* **44**, 165-178.e166. doi:10.1016/j.devcel.2017.12.004

Ihn, H., Ihn, Y. and Trojanowska, M. (2001). Sp1 phosphorylation induced by serum stimulates the human alpha2(I) collagen gene expression. *J. Invest. Dermatol.* **117**, 301-308. doi:10.1046/j.0022-202x.2001.01371.x

Jamora, C., DasGupta, R., Kocieniewski, P. and Fuchs, E. (2003). Links between signal transduction, transcription and adhesion in epithelial bud development. *Nature* **422**, 317-322. doi:10.1038/nature01458

Järvinen, E., Salazar-Ciudad, I., Birchmeier, W., Taketo, M. M., Jernvall, J. and Thesleff, I. (2006). Continuous tooth generation in mouse is induced by activated epithelial Wnt/beta-catenin signaling. *Proc. Natl. Acad. Sci. U.S.A.* **103**, 18627-18632. doi:10.1073/pnas.0607289103

Jarvinen, E., Shimomura-Kuroki, J., Balic, A., Jussila, M. and Thesleff, I. (2018). Mesenchymal Wnt/beta-catenin signaling limits tooth number. *Development* **145**, dev158048. doi:10.1242/dev.158048

Kozawa, Y., Yokota, R., Chisaka, H., Yamamoto, H., Suzuki, K. and Elsey, R. M. (2005). Evagination and invagination of the oral epithelium during tooth development in alligator mississippiensis. *J. Hard Tissue Biol.* **14**, 170-171. doi:10.2485/jhtb.14.170

Lammi, L., Arte, S., Somer, M., Järvinen, H., Lahermo, P., Thesleff, I., Pirinen, S. and Nieminen, P. (2004). Mutations in AXIN2 cause familial tooth agenesis and predispose to colorectal cancer. *Am. J. Hum. Genet.* **74**, 1043-1050. doi:10.1086/386293

Li, J., Chatzeli, L., Panousopoulou, E., Tucker, A. S. and Green, J. B. A. (2016). Epithelial stratification and placode invagination are separable functions in early morphogenesis of the molar tooth. *Development* **143**, 670-681. doi:10.1242/dev.130187

Liu, F., Chu, E. Y., Watt, B., Zhang, Y., Gallant, N. M., Andl, T., Yang, S. H., Lu, M. M., Piccolo, S., Schmidt-Ullrich, R. et al. (2008). Wnt/beta-catenin signaling directs multiple stages of tooth morphogenesis. *Dev. Biol.* **313**, 210-224. doi:10.1016/j.ydbio.2007.10.016

Liu, W., Shaver, T. M., Balasa, A., Ljungberg, M. C., Wang, X., Wen, S., Nguyen, H. and Van den Veyver, I. B. (2012). Deletion of Porcn in mice leads to multiple developmental defects and models human focal dermal hypoplasia (Goltz syndrome). *PLoS ONE* **7**, e32331. doi:10.1371/journal.pone.0032331

Mammoto, T., Mammoto, A., Jiang, A., Jiang, E., Hashmi, B. and Ingber, D. E. (2015). Mesenchymal condensation-dependent accumulation of collagen VI stabilizes organ-specific cell fates during embryonic tooth formation. *Dev. Dyn.* **244**, 713-723. doi:10.1002/dvdy.24264

Metscher, B. D. (2009). MicroCT for comparative morphology: simple staining methods allow high-contrast 3D imaging of diverse non-mineralized animal tissues. *BMC Physiol.* **9**, 11. doi:10.1186/1472-6793-9-11

Murray, J. D. and Kulesa, P. M. (1996). On a dynamic reaction–diffusion mechanism: the spatial patterning of teeth primordia in the alligator. *J. Chem. Soc. Faraday Trans.* **92**, 2927-2932. doi:10.1039/FT9969202927

Panousopoulou, E. and Green, J. B. (2016). Invagination of ectodermal placodes is driven by cell intercalation-mediated contraction of the suprabasal tissue canopy. *PLoS Biol.* **14**, e1002405. doi:10.1371/journal.pbio.1002405

Prochazka, J., Prochazkova, M., Du, W., Spoutil, F., Tureckova, J., Hoch, R., Shimogori, T., Sedlacek, R., Rubenstein, J. L., Wittmann, T. et al. (2015). Migration of founder epithelial cells drives proper molar tooth positioning and morphogenesis. *Dev. Cell* **35**, 713-724. doi:10.1016/j.devcel.2015.11.025

Riddle, R. D., Johnson, R. L., Laufer, E. and Tabin, C. (1993). Sonic hedgehog mediates the polarizing activity of the ZPA. *Cell* **75**, 1401-1416. doi:10.1016/0092-8674(93)90626-2

Sadier, A., Twarogowska, M., Steklikova, K., Hayden, L., Lambert, A., Schneider, P., Laudet, V., Hovorakova, M., Calvez, V. and Pantalacci, S. (2019). Modeling Edar expression reveals the hidden dynamics of tooth signaling center patterning. *PLoS Biol.* **17**, e3000064. doi:10.1371/journal.pbio.3000064

Sasaki, T., Ito, Y., Xu, X., Han, J., Bringas, P., Jr., Maeda, T., Slavkin, H. C., Grosschedl, R. and Chai, Y. (2005). LEF1 is a critical epithelial survival factor during tooth morphogenesis. *Dev. Biol.* **278**, 130-143. doi:10.1016/j.ydbio.2004.10.021

Shyer, A. E., Rodrigues, A. R., Schroeder, G. G., Kassianidou, E., Kumar, S. and Harland, R. M. (2017). Emergent cellular self-organization and mechanosensation initiate follicle pattern in the avian skin. *Science* **357**, 811-815. doi:10.1126/science.aai7868

Sick, S., Reinker, S., Timmer, J. and Schlake, T. (2006). WNT and DKK determine hair follicle spacing through a reaction-diffusion mechanism. *Science* **314**, 1447-1450. doi:10.1126/science.1130088

Smith, M. M., Johanson, Z., Butts, T., Ericsson, R., Modrell, M., Tulenko, F. J., Davis, M. C. and Fraser, G. J. (2015). Making teeth to order: conserved genes reveal an ancient molecular pattern in paddlefish (Actinopterygii). *Proc. Biol. Sci.* **282**, 20142700. doi:10.1098/rspb.2014.2700

Stricker, J., Falzone, T. and Gardel, M. L. (2010). Mechanics of the F-actin cytoskeleton. *J. Biomech.* **43**, 9-14. doi:10.1016/j.jbiomech.2009.09.003

ten Berge, D., Koole, W., Fuerer, C., Fish, M., Eroglu, E. and Nusse, R. (2008). Wnt signaling mediates self-organization and axis formation in embryoid bodies. *Cell Stem Cell* **3**, 508-518. doi:10.1016/j.stem.2008.09.013

Thesleff, I. and Sharpe, P. (1997). Signalling networks regulating dental development. *Mech. Dev.* **67**, 111-123. doi:10.1016/S0925-4773(97)00115-9

Tokita, M., Chaeychomsri, W. and Siruntawineti, J. (2013). Developmental basis of toothlessness in turtles: insight into convergent evolution of vertebrate morphology. *Evolution* **67**, 260-273. doi:10.1111/j.1558-5646.2012.01752.x

DEVELOPMENT

Tucker, A. S. and Sharpe, P. T. (1999). Molecular genetics of tooth morphogenesis and patterning: the right shape in the right place. *J. Dent. Res.* **78**, 826-834. doi:10.1177/00220345990780040201

Valenta, T., Hausmann, G. and Basler, K. (2012). The many faces and functions of beta-catenin. *EMBO J.* **31**, 2714-2736. doi:10.1038/emboj.2012.150

van Roy, F. and Berx, G. (2008). The cell-cell adhesion molecule E-cadherin. *Cell. Mol. Life Sci.* **65**, 3756-3788. doi:10.1007/s00018-008-8281-1

Wang, X. P. and Fan, J. (2011). Molecular genetics of supernumerary tooth formation. *Genesis* **49**, 261-277. doi:10.1002/dvg.20715

Wang, X.-P., O'Connell, D. J., Lund, J. J., Saadi, I., Kuraguchi, M., Turbe-Doan, A., Cavallesco, R., Kim, H., Park, P. J., Harada, H. et al. (2009). Apc inhibition of Wnt signaling regulates supernumerary tooth formation during embryogenesis and throughout adulthood. *Development* **136**, 1939-1949. doi:10.1242/dev.033803

Widelitz, R. B., Jiang, T. X., Yu, M., Shen, T., Shen, J. Y., Wu, P., Yu, Z. and Chuong, C.-M. et al. (2003). Molecular biology of feather morphogenesis: a testable model for evo-devo research. *J. Exp. Zool. B Mol. Dev. Evol.* **298**, 109-122. doi:10.1002/jez.b.29

Yu, T. and Klein, O. D. (2020). Molecular and cellular mechanisms of tooth development, homeostasis and repair. *Development* **147**, dev184754. doi:10.1242/dev.184754

DEVELOPMENT